Supporting Information:

Conformal Ultrathin Film MOF Analogs: Characterization of Growth, Porosity, and Electronic Transport

Jonathan Lau,[†] Ashley E. Trojniak,[§] Macy J. Maraugha,[§] Alyssa J. VanZanten,[§] Alexander J. Osterbaan,[§] Andrew C. Serino,[†] Monica L. Ohnsorg,[§] Kevin M. Cheung,[‡,#] David S. Ashby,[†] Paul S. Weiss,[†,‡,#] Bruce S. Dunn,[†,#] and Mary E. Anderson[§,¥,*]

[†]Department of Materials Science and Engineering, University of California, Los Angeles, Los Angeles, California 90095, United States

[‡]Department of Chemistry and Biochemistry, University of California, Los Angeles, Los Angeles, California 90095, United States

[#]California NanoSystems Institute, University of California, Los Angeles, Los Angeles, California 90095, United States

[§]Department of Chemistry, Hope College, Holland, Michigan 49423, United States

[¥]Department of Chemistry, Furman University, Greenville, South Carolina, 29613, United States

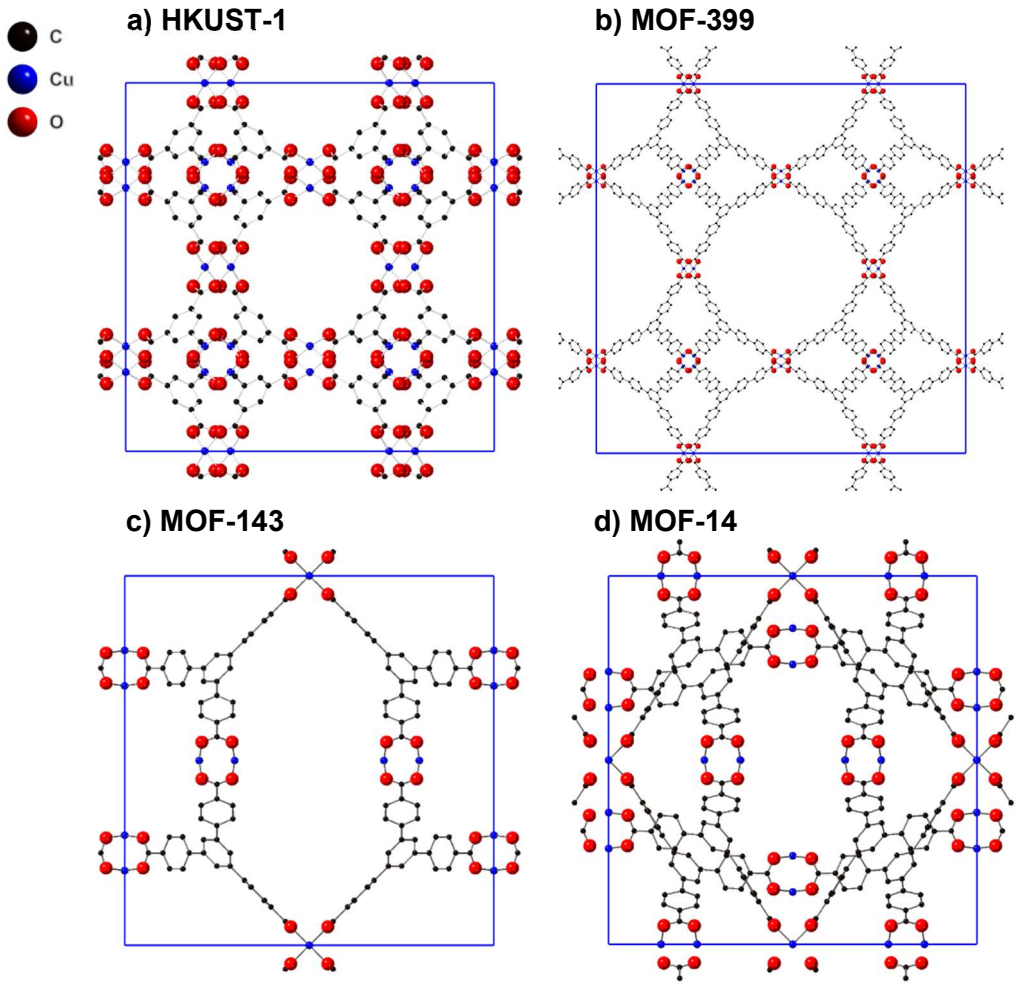

Figure S1. Crystal structures for (a) HKUST-1,[S1] (b) MOF-399,[S2] (c) MOF-143,[S2] and (d) MOF-14.[S3] These MOFs are all composed of copper paddlewheel nodes with tritopic ligands and represent two types of topology: HKUST-1 and MOF-399 are tbo and MOF-143 and MOF-14 are pto. MOF-143 and MOF-14 are composed of the same inorganic and organic compounds, but MOF-14 has a higher density than MOF-143. This is because MOF-14 structure is composed of two MOF-143 interpenetrating structures.

These structures were rendered using CrystalMaker software from .cif files made available as Supporting Information associated with refs (S1-S3).

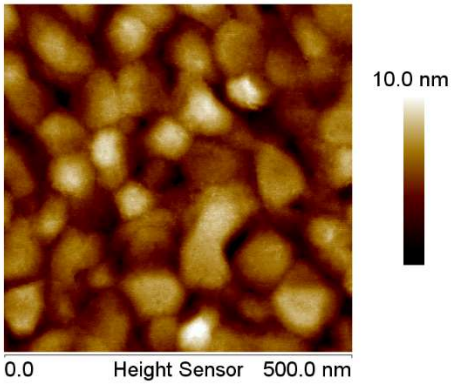

Figure S2. Representative atomic force microscopy (AFM) image (500 nm × 500 nm) of a gold substrate after deposition of a 16-mercaptohexadecanoic acid SAM. The roughness (Rq) was measured to be 1.55 nm.

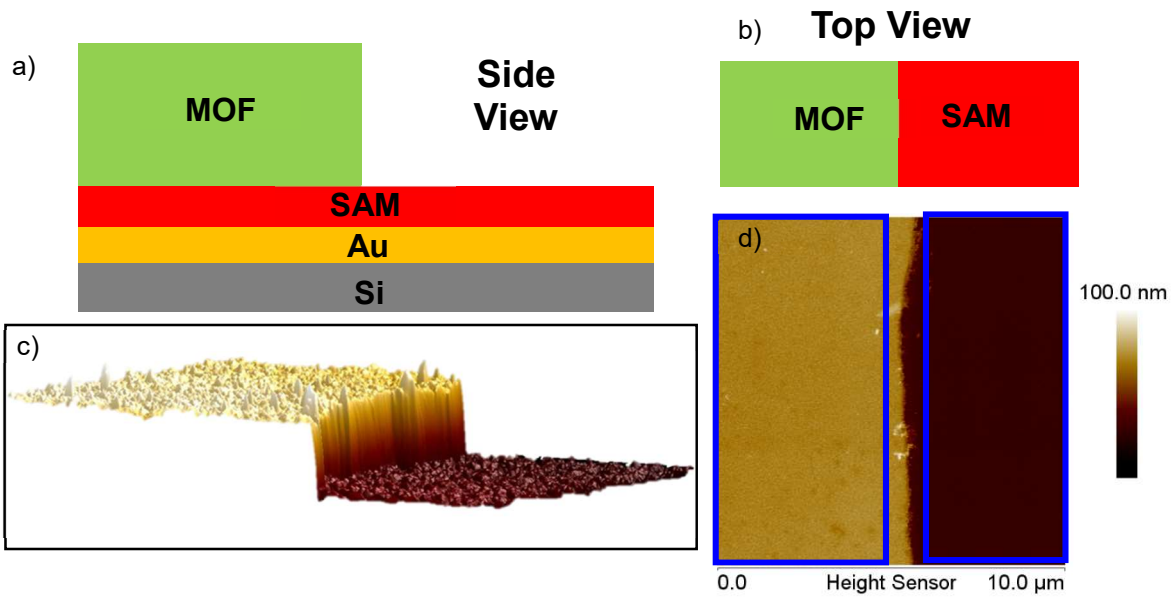

Figure S3. (a,b) Schematic representing the step edge of a metal-organic framework (MOF) film relative to the Au substrate after selective etching. Representative atomic force microscopy (AFM) image (10 µm × 10 µm) for MOF-399 film after etching, with (c) side view and (d) top view three-dimensional renderings. The blue rectangles in (d) represent the selected regions in which the average height was calculated and the difference between the two is the MOF film thickness.

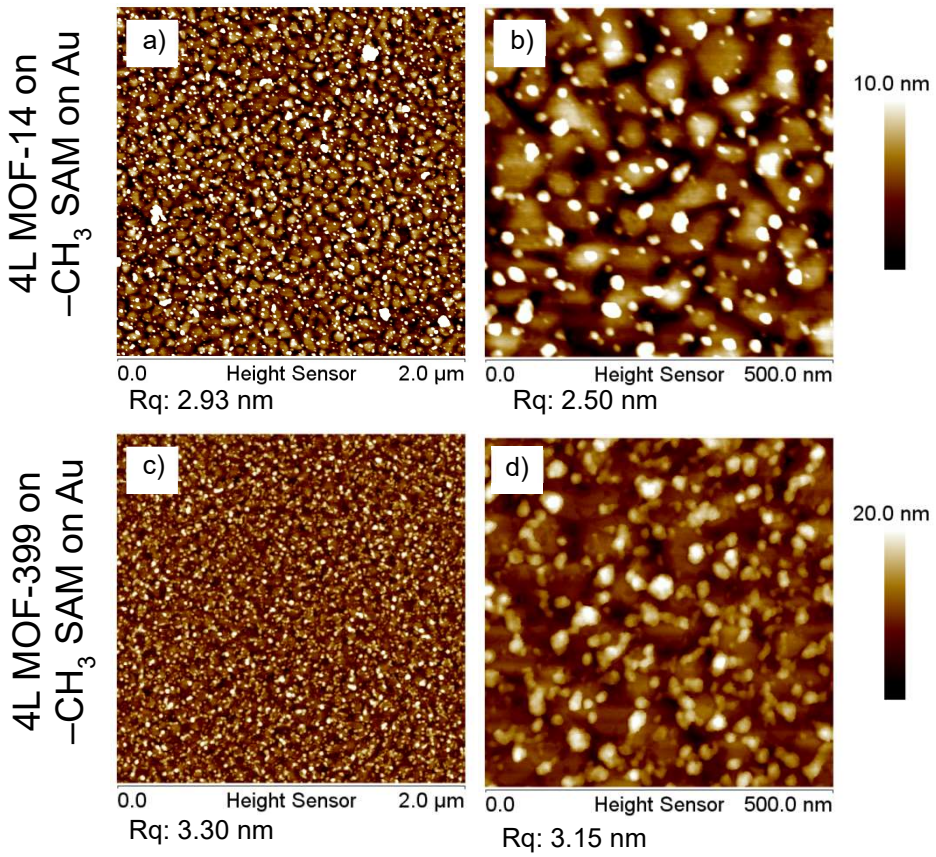

Figure S4. Representative atomic force microscopy images (left column: 2 µm × 2 µm, right column: 500 nm × 500 nm) for (a,b) 4L MOF-14 and (c,d) 4L MOF-399 films deposited on a methyl-terminated octadecanethiol self-assembled monolayer. Below each image, the roughness (R_q) is given.

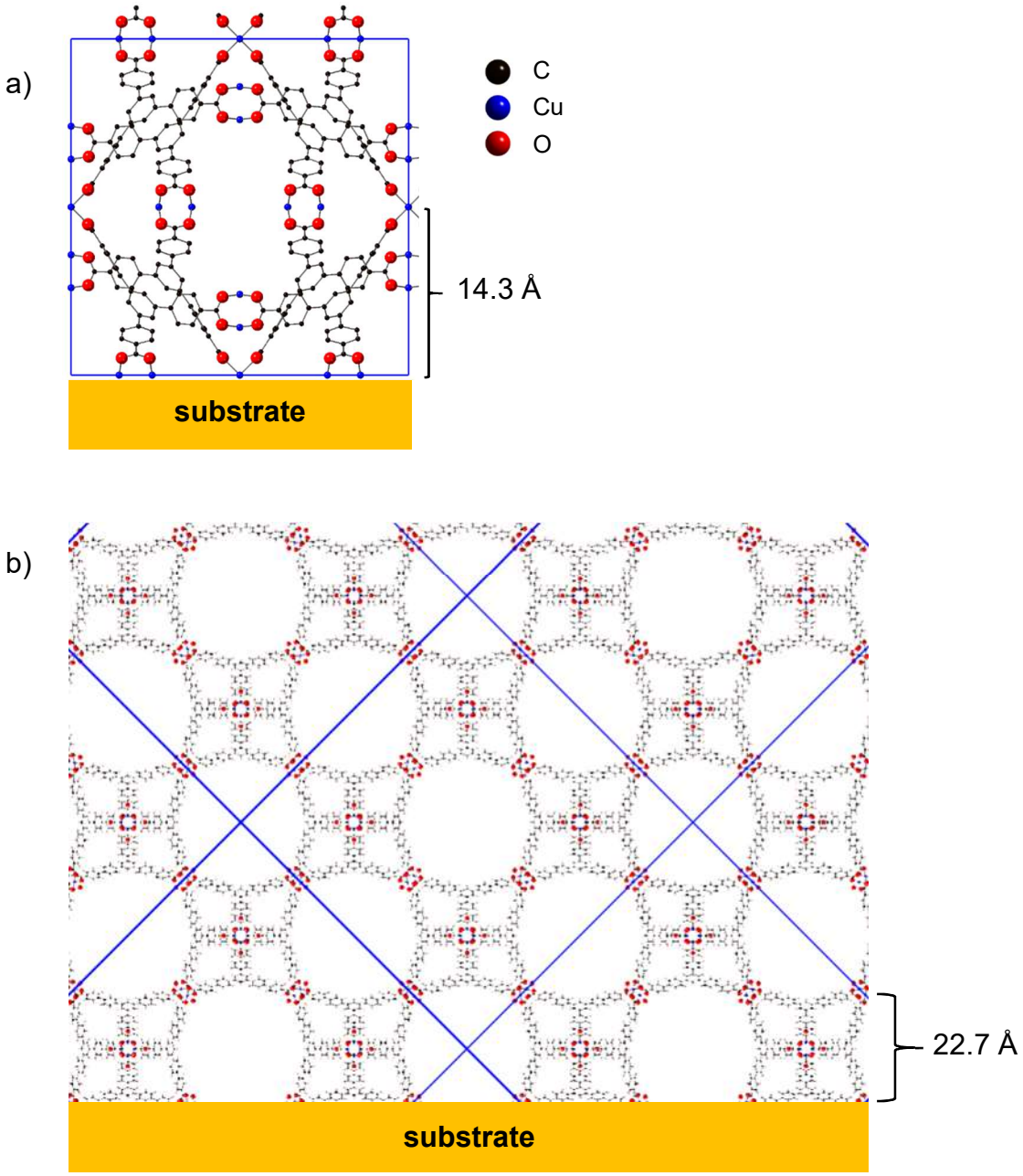

Figure S5. Schematic of the hypothesized structures of the films for the (a) MOF-14-based and (b) MOF-399-based systems. These are proposed based on unit cell dimensions, dimensions of the organic ligands, and film thickness per deposition cycle. The {100} face of the cubic unit cells are shown with single unit cell outlined in blue. The edge of the unit cell for MOF-14 is 26.9 Å and 68.3 Å for MOF-399.[S2,S3] The thickness indicated to the right of the MOF structures represents the triangular edge length of the tritopic ligand from one carboxylic acid to the copper coordinated on another carboxylic acid. This corresponds well with the film thickness increase per deposition cycle of 14 Å and 22 Å for MOF-14 and MOF-399 analogs, respectively.

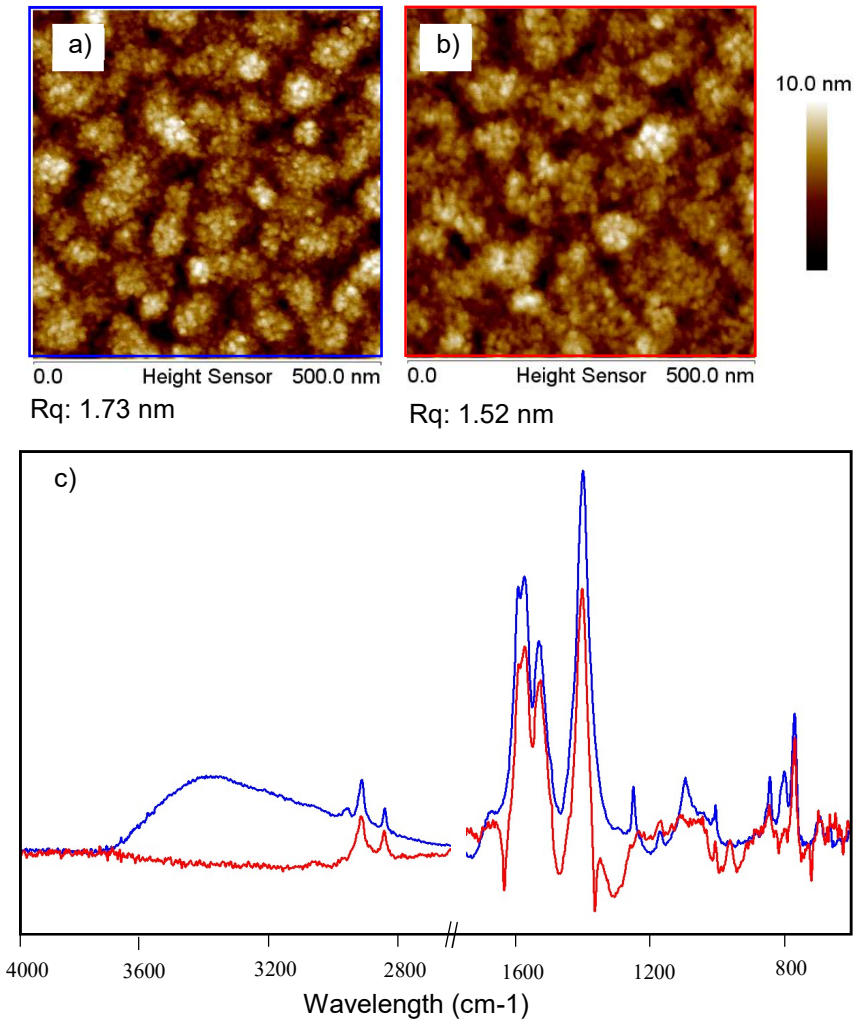

Figure S6. Representative atomic force microscopy images (500 nm × 500 nm) for a 4L MOF-14 film (a) before and (b) after heating to 200 °C for 2 h with film roughness (Rq) listed below each image. (c) Representative IR spectra for these samples showing removal of the water peak from 3600-3000 cm^{-1} after heating.

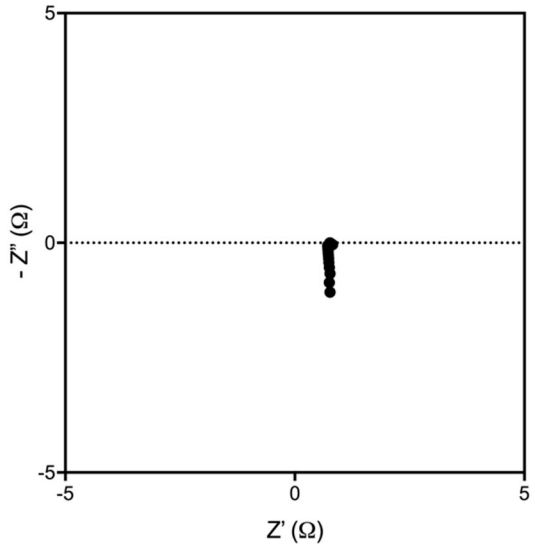

Figure S7. Electrochemical impedance spectroscopy (EIS) spectra of the hanging mercury drop electrode (HMDE) electrically short-circuited to a stainless steel electrode. The use of the HMDE does not introduce a large resistance to the impedance measurement. The HMDE electrically short-circuited to a bare Au substrate displays a similar resistance.

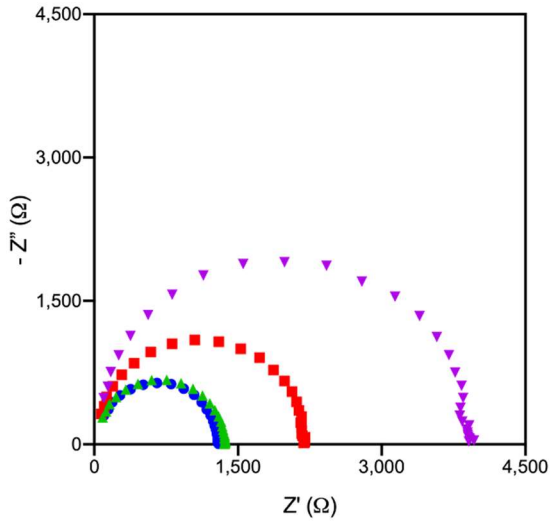

Figure S8. Electrochemical impedance spectroscopy (EIS) of an 8L MOF-14 film after heating. The spectra represent measurements on different positions of the film. The spread in the impedance is due to the range of hanging mercury drop electrode (HMDE) contact areas (from 1-3 mm in diameter) that can vary depending on the distance between the HMDE and the sample. The average parallel resistance obtained from equivalent circuit fitting is used to calculate the electrical conductivity for SurMOF films of the MOF-14 system. The EIS spectrum with parallel resistance close to the average value was selected for inclusion within the manuscript (Figure 5).

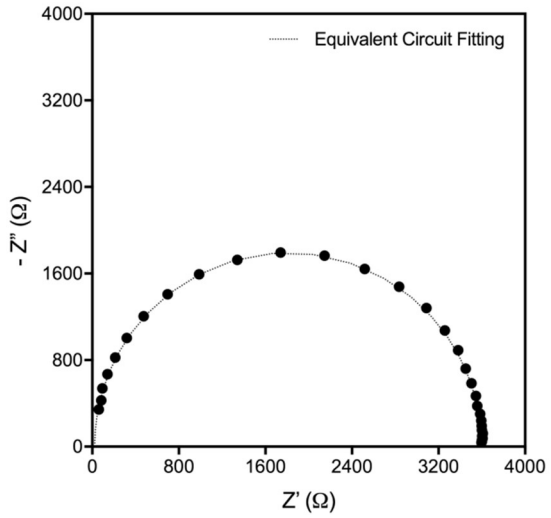

Figure S9. Representative electrochemical impedance spectra of a 12L MOF-14 film after 1 h of anhydrous dimethyl sulfoxide vapor treatment.

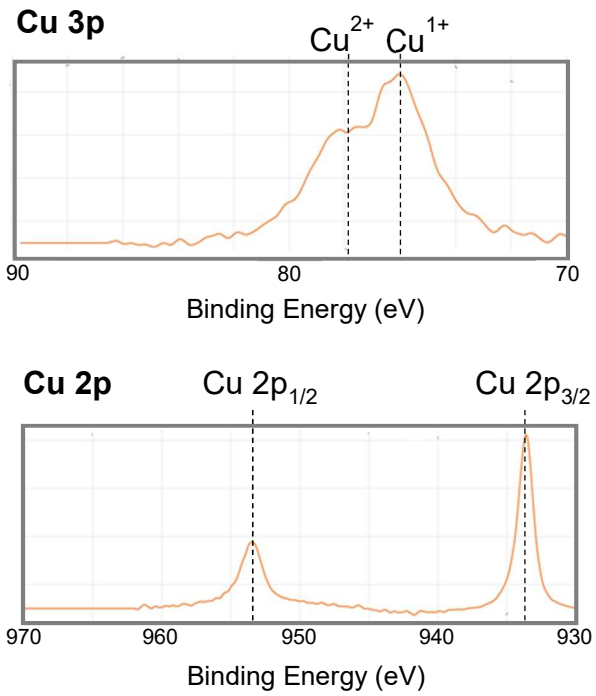

Figure S10. Representative high-resolution X-ray photoelectron spectroscopy (XPS) spectra of a 12L MOF-399 film showing the two oxidation states of copper within the film. The presence of the two oxidation states is common as Cu^{2+} is known to reduce to Cu^{1+} during XPS measurements of ultrathin metal-organic coordinated multilayer films.[S4,S5]

Calculated Diffusion Coefficient

The diffusion coefficient, D, of Fc in the 10 mM ferrocene (Fc)|100 mM tetrabutylammonium tetrafluoroborate (TBATFB) in propylene carbonate (PC) electrolyte was calculated from cyclic voltammograms with a bare Au working electrode and using the Randles-Sevcik equation (Equation 1) where i_p is the redox peak current (oxidative peak currents used for consistency), n is the number of electrons transferred in the redox reaction, F is the Faraday constant, A is the electrode area, C is the concentration of the redox couple, v is the sweep rate, and R is the gas constant. The diffusion coefficient of a redox molecule can be extracted from the slope of the peak currents vs the square-root of the sweep rate.

$$i_p = 0.4463nFAC\left(\frac{nFvD}{RT}\right)^{\frac{1}{2}} \qquad \text{Equation 1}$$

The solvation shell diameter of the diffusing species, d, was calculated using the diffusion coefficient of Fc using the Stokes-Einstein equation (Equation 2) where k_B is the Boltzmann constant and η is viscosity of the electrolyte (approximated by pure PC).

$$D = \frac{k_B T}{3\pi\eta d} \qquad \text{Equation 2}$$

The diffusion coefficient of Fc in PC is determined to be 1.6×10^{-6} cm^2 s^{-1}, resulting in a solvation shell diameter of 1.1 nm.

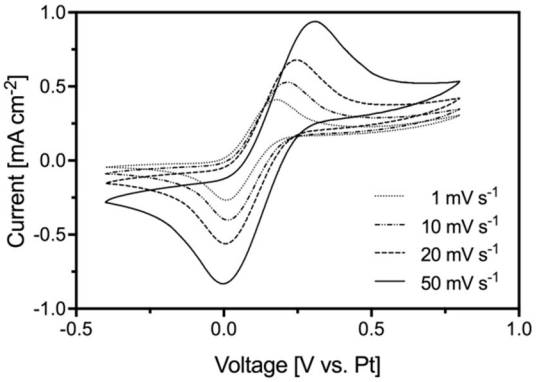

Figure S11. Cyclic voltammetry of a bare Au substrate cycled in 10 mM ferrocene|100 mM tetrabutylammonium tetrafluoroborate in propylene carbonate at sweep rates of 1, 10, 20, and 50 mV s^{-1}.

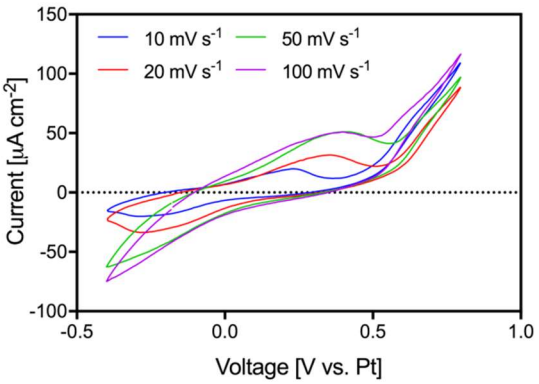

Figure S12. Cyclic voltammetry of a 8L MOF-399 film cycled in 10 mM ferrocene|100 mM tetrabutylammonium tetrafluoroborate in propylene carbonate at sweep rates of 10, 20, 50, and 100 mV s^{-1}. Peak currents are expected to be proportional to the square-root of the sweep rate for linear diffusion (3× expected increase in current from 10 mV s^{-1} to 100 mV s^{-1}). The saturation of the peak current at 100 mV s^{-1} provides further evidence that the linear diffusion of Fc due to macroscopic defects is not responsible for the redox peaks observed.

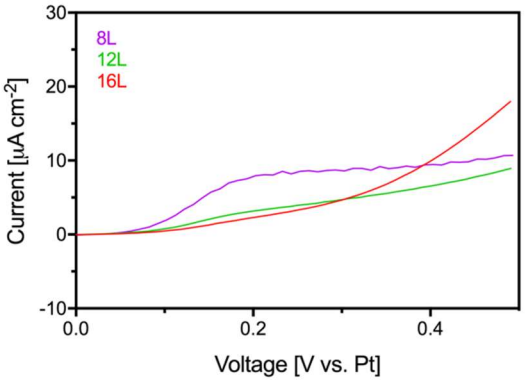

Figure S13. Comparison of oxidative currents for 8L, 12L, and 16L MOF-14 films cycled in 10 mM ferrocene|100 mM tetrabutylammonium tetrafluoroborate in propylene carbonate measured using cyclic voltammetry at a sweep rate of 10 mV s^{-1}.

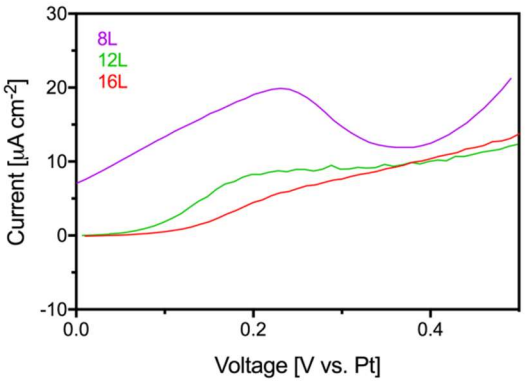

Figure S14. Comparison of oxidative currents for 8L, 12L, and 16L MOF-399 films cycled in 10 mM ferrocene|100 mM tetrabutylammonium tetrafluoroborate in propylene carbonate measured using cyclic voltammetry at a sweep rate of 10 mV s^{-1}.

Table S1. Oxidative currents in μA cm^{-2} at the oxidation potential of ferrocene for MOF-14 and MOF-399 films in 10 mM ferrocene |100 mM tetrabutylammonium tetrafluoroborate in propylene carbonate measured using cyclic voltammetry at a sweep rate of 10 mV s^{-1}.

Thickness (# layers)	MOF-14	MOF-399
8 L	8.5	19.3
12 L	3.9	8.9
16 L	3.3	6.4

References:

(S1) Chui, S. S.-Y.; Lo, S. M.-F.; Charmant, J. P. H.; Orpen, A. G.; Williams, I. D. A Chemically Functionalizable Nanoporous Material $[Cu_3(TMA)_2(H_2O)_3]_n$. *Science* **1999**, *283*, 1148–1150.

(S2) Furukawa, H.; Go, Y. B.; Ko, N.; Park, Y. K.; Uribe-Romo, F. J.; Kim, J.; O'Keeffe, M.; Yaghi, O. M. Isoreticular Expansion of Metal-Organic Frameworks with Triangular and Square Building Units and the Lowest Calculated Density for Porous Crystals. *Inorganic Chemistry* **2011**, *50*, 9147–9152.

(S3) Eddaoudi, M.; Kim, J.; Rosi, N.; Vodak, D.; Wachter, J.; O'Keeffe, M.; Yaghi, O. M. Systematic Design of Pore Size and Functionality in Isoreticular MOFs and Their Application in Methane Storage. *Science* **2002**, *295*, 469–472.

(S4) Freeman, T. L.; Evans, S. D.; Ulman, A. XPS Studies of Self-Assembled Multilayer Films, *Langmuir* **1995**, *11*, 4411–4417.

(S5) Daniel, T. A.; Uppili, S.; McCarty, G. ; Allara, D. L. Effects of Molecular Structure and Interfacial Ligation on the Precision of Cu-Bound α,ω-Mercaptoalkanoic Acid "Molecular Ruler" Stacks, *Langmuir* **2007**, *23*, 638–648.